New read-out electronics for ICARUS-T600 liquid argon TPC. Description, simulation and tests of the new front-end and ADC system

Published by IOP Publishing for Sissa Medialab

Received: *May 14, 2018*
Revised: *September 25, 2018*
Accepted: *October 31, 2018*
Published: *December 4, 2018*

New read-out electronics for ICARUS-T600 liquid argon TPC. Description, simulation and tests of the new front-end and ADC system

The ICARUS/NP01 collaboration

L. Bagby,[a] B. Baibussinov,[b] V. Bellini,[c] M. Bonesini,[d] A. Braggiotti,[b,e] L. Castellani,[b] S. Centro,[b] T. Cervi,[f] A.G. Cocco,[g] F. Fabris,[b] A. Falcone,[f,1] C. Farnese,[b,2] A. Fava,[a,b] F. Fichera,[c] D. Franciotti,[h] G. Galet,[b] D. Gibin,[b] A. Guglielmi,[b] R. Guida,[b] W. Ketchum,[a] S. Marchini,[b] A. Menegolli,[f] G. Meng,[b] G. Menon,[b] C. Montanari,[f,a] M. Nessi,[i] M. Nicoletto,[b] R. Pedrotta,[b] P. Picchi,[f] F. Pietropaolo,[b,i] G. Rampazzo,[b] A. Rappoldi,[f] G.L. Raselli,[f] M. Rossella,[f] C. Rubbia,[h,i,j,3] A. Scaramelli,[f] F. Sergiampietri,[k] M. Spanu,[f] M. Torti,[d] F. Tortorici,[c] F. Varanini,[b] S. Ventura,[b] C. Vignoli,[h] A. Zani[i] and P.G. Zatti[b]

[a] *Fermi National Accelerator Laboratory, Batavia, Illinois, U.S.A.*
[b] *Dipartimento di Fisica e Astronomia "G. Galilei", Università di Padova and INFN, Padova, Italy*
[c] *Dipartimento di Fisica e Astronomia, Università di Catania and INFN, Catania, Italy*
[d] *Dipartimento di Fisica "G. Occhialini", Università di Milano-Bicocca and INFN Milano-Bicocca, Milano, Italy*
[e] *Istituto di Neuroscienze, CNR, Padova, Italy*
[f] *Dipartimento di Fisica, Università di Pavia and INFN, Pavia, Italy*
[g] *Dipartimento di Scienze Fisiche, Università Federico II di Napoli and INFN, Napoli, Italy*
[h] *INFN – Laboratori Nazionali del Gran Sasso, Assergi, Italy*
[i] *CERN, Geneva, Switzerland*
[j] *GSSI, L'Aquila, Italy*
[k] *INFN, Pisa, Italy*

E-mail: christian.farnese@pd.infn.it

Abstract: The ICARUS T600, a liquid argon time projection chamber (LAr-TPC) detector mainly devoted to neutrino physics, underwent a major overhauling at CERN in 2016–2017, which included also a new design of the read-out electronics, in view of its operation in Fermilab on the Short Baseline Neutrino (SBN) beam from 2019. The new more compact electronics showed capability of handling more efficiently the signals also in the intermediate Induction-2 wire plane with a

[1] Now at University of Texas, Arlington, Texas, U.S.A..
[2] Corresponding author.
[3] Spokesperson.

https://doi.org/10.1088/1748-0221/13/12/P12007

2018 JINST 13 P12007

significant increase of signal to noise (S/N), allowing for charge measurement also in this view. The new front-end and the analog to digital conversion (ADC) system are presented together with the results of the tests on 50 liters liquid argon TPC performed at CERN with cosmic rays.

KEYWORDS: Front-end electronics for detector readout; Neutrino detectors; Noble liquid detectors (scintillation, ionization, double-phase); Time projection Chambers (TPC)

ARXIV EPRINT: 1805.03931

2018 JINST 13 P12007

Contents

2018 JINST 13 P12007

1 Introduction

The LAr-TPC, a detection technique that allows for accurately identifying and reconstructing each ionizing track, has been proposed in 1977 [1] as alternative to Cerenkov radiation detectors. With the continue effort of ICARUS Collaboration and INFN support, the LAr-TPC technique has been taken to the full maturity with the LAr large mass T600 detector successfully operated in 2010–2013 at the LNGS underground laboratories exposed to CNGS beam and cosmic rays with a live-time $> 93\%$ [2].

The ICARUS T600 detector consists of a large cryostat split into two identical, adjacent half-modules with internal dimensions $3.6 \times 3.9 \times 19.6\,\mathrm{m}^3$ and filled with about 760 tons of ultra-pure liquid Argon continuously purified to prevent absorption of ionization electrons by electronegative elements [3]. A uniform electric field ($\mathrm{E}_D = 500$ V/cm) is applied to the LAr bulk: each half-module houses two TPCs separated by a common cathode. Charged particles, generated for example by a neutrino crossing the medium and interacting in LAr, produce ionization along their path. Thanks to the low transverse diffusion of charge in LAr, the electron images of ionization tracks are preserved and, drifting along the electric field lines, are projected onto the anode (TPC) — see the illustration in figure 1. Each TPC is made of three parallel planes of wires, 3 mm apart, facing the drift path (1.5 m). The wire pitch is also 3 mm. Globally, 53248 wires with length up to 9 m are installed in the detector. By appropriate voltage biasing, the first two planes (Induction-1 and Induction-2 planes) are transparent to charge and provide signals in non-destructive way (induced signals), whereas the ionization charge is finally fully collected by the last one (Collection plane). Wires are oriented on each plane at a different angles ($0°$, $+60°$, $-60°$) with respect to the horizontal direction. Therefore, combining the wire coordinate on each plane at a given drift time, a three-dimensional image of the ionizing event can be reconstructed. Moreover, the charge signal detected in the Collection view, proportional to the deposited energy, allows for the calorimetric measurement of the particle energy. A remarkable resolution of about $1\,\mathrm{mm}^3$ is uniformly achieved over the whole detector active volume ($\sim 340\,\mathrm{m}^3$). The measurement of the absolute time of the ionizing event, detecting scintillation light with an arrays of Photo Multiplier Tubes (PMTs) [4], combined with the electron

drift velocity information ($v_D \sim 1.6$ mm/μs at $E_D = 500$ V/cm), provides the absolute position of the track along the drift coordinate. The electronics was designed to allow for continuous read-out, digitization and independent waveform recording of signals from each wire of the TPC. The read-out chain is organized on a 32-channel modularity. A Decoupling Board receives the signals from the chamber and passes them to an Analogue Board via decoupling capacitors; it also provides wire biasing voltage and the distribution of the test signals. The Analogue Board hosts the front-end amplifiers and performs 16:1 channel multiplexing and 10-bit ADC digitization at 400 ns sampling time per channel. The overall gain is about 1000 electrons per ADC count, setting the signal of minimum ionizing particles to ~ 15 ADC counts with a dynamic range of about 100 minimum ionizing particles taking into account ~ 15000 free electrons produced by a minimum ionizing particle in 3 mm.

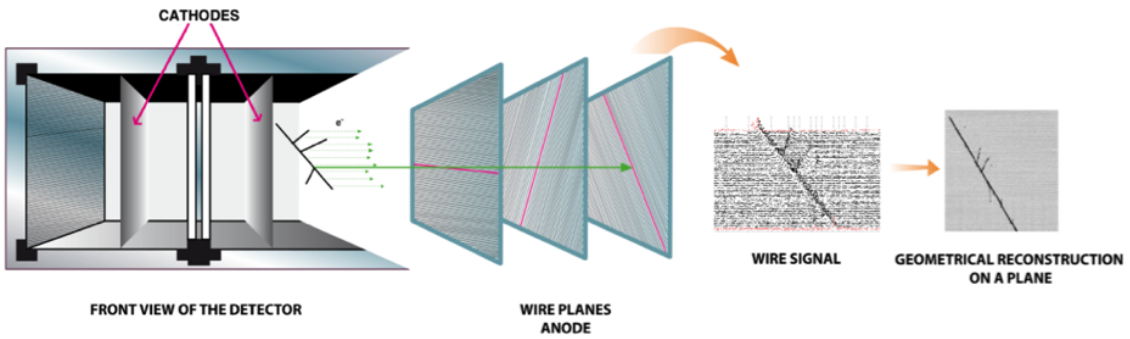

Figure 1. Sketch of detector layout showing the LAr TPC working mechanism.

For the front-end amplifier a 3 μs decay constant was used for the unipolar signals coming from Collection and Induction-1 wires, while 100 μs decay constant was used for the bipolar current signals (Induction-2 wires). The front-integrator was followed by a baseline restorer to reduce the low frequency noise acting as instability of the signal baseline. The aim was to shape the bipolar Induction-2 signal in a way to make it appears as unipolar. For isolated tracks it worked fine. However, there were serious limitations with signals produced by the intermediate Induction-2 wire plane in case of showers extending along the drift coordinate over a time interval comparable to the decay constant of the preamplifier chain, leading to sizable variation of the baseline (undershoot) which in turn made the shower reconstruction difficult, mainly for energy measurement. A Digital Board hosts a 10 bit wide, waveform recorder. It continuously reads the data, stores them in multi-event circular buffers, each covering a full drift distance. When a trigger signal occurs, the active buffer is frozen, writing operations are moved to the next free buffer, and the stored data are read out by the DAQ. This configuration guarantees no dead time, until the maximum DAQ throughput (1 full-drift event per second) is reached. The average electronic noise achieved with the special designed low noise front-end is well within expectations: 1500 electrons r.m.s. to be compared with ~ 15000 free electrons produced by a minimum ionizing particle in 3 mm (S/N ~ 10).

A detailed description of the ICARUS detector can be found elsewhere [5].

The three years long run of Icarus at LNGS demonstrated its remarkable event identification and measurement capabilities investigating the presence of the LSND-like ν_μ–ν_e oscillations in the CNGS neutrino beam [6]. Moreover a sample of atmospheric neutrino interactions in the 0.2–2 GeV

2018 JINST 13 P12007

energy range was collected to qualify the detector performance in the energy range of interest for the forthcoming operation of ICARUS-T600 in the SBN program at Fermilab aiming to definitely clarify the LSND effect [7].

The ICARUS front-end amplifier and multiplexed ADC system, used in the LNGS run, performed efficiently with an extremely good S/N ratio that allowed for collecting some thousands neutrino and cosmic events with unprecedented quality. However, the signal shaping chosen at the time presented some limitations on signals produced by the intermediate Induction-2 wire plane in case of dense showers. The overhauling of ICARUS T600 performed at CERN in preparation for its operation at Fermilab, gave the opportunity of designing new electronics, which integrates the DAQ boards onto the signal flanges. Moreover, overhauling gave the opportunity of designing a new more compact front-end amplifier with a different signal shaping. This new design showed to be capable of handling more efficiently also the Induction-2 signals, with a significant increase of S/N allowing for measurement of deposited energy also in this view. In this paper, the new front-end and the AD conversion system will be presented together with results of the tests performed at CERN with the 50 liters liquid argon LAr-TPC [8].

The DAQ of T600 was conceived in 1997 and front-end dual channel BiCMOS circuits were designed in 1998. The full system was designed and built from 1999 to 2000 and operated first time in 2001. The integration of a new electronics onto the flanges will drastically reduce the cost and occupancy thanks of use of new more advanced components. One evident limitation of T600 DAQ was due to the choice of the VME standard (8–10 MB/s), perfectly legitimate at that time. The digital part is not described in detail in this paper however an architecture that dedicates to each channel an ADC (12 bit, 400 ns sampling), avoiding multiplexing, and treats the digital stream with a single powerful FPGA, controlling the memory buffers and driving optical link, will allow for higher data rates (1 Gbit/s) and simplifying the system. Basically the full system saves the old architecture and behaves as a waveform recorder, with digital buffers, for each wire of the detector.

2 Amplifier architecture

The adopted architecture is the same of the original design [5]: a Radeka-like amplifier with 3 parallel jFet as input stage, followed by an unfolded cascode integrated in a dual channel BiCMOS ASIC, CCA2C in figure 2. Multiple jFet (BF861C) at input, were adopted to achieve a total g_m in the order of 45 mS. The total drain current (about 12.5 mA) is set by high accuracy resistors R9 and R10 connected between the regulated +7 V power supply and the drain which voltage is precisely defined by the unfolded cascade stage inside the monolithic circuit. This stage, while mitigates the Miller effect, fully collects the drain current modulated by the signal, due to its extremely low impedance. The capacitance in front of the amplifier is due to the cables length ($\sim$ 4–5 m, 50 pF/m) and wires capacitance ($\sim$ 9 m, 20 pF/m). The total capacitance is always in the order of 400 pF, that means the serial noise is dominant and its effect must be mitigated by high transconductance at input stage. The ASIC (CCA2C) custom design was chosen for performance uniformity and compactness. To improve this latter a new even smaller custom package ($4 \times 4\,\mathrm{mm}^2$) was chosen. The input stage is, in this new design, followed by a shaper (a classic pole-zero cancellation filter performed by U1A) and baseline restorer with a peaking time of 0.6 µs in response of a delta-like input current at zero detector capacitance. This choice will eliminate the problem faced in case of

2018 JINST 13 P12007

bipolar signals as in Induction-2. In fact, as already mentioned, signals generated by dense particle showers, with a time extension comparable with the 100 µs long time constant of the old front-end electronics, caused large undershoots masking the signal fine structure. The basic scheme of the new front end is given in figure 3.

The same shaping time was chosen both for Induction and Collection signals. In this way, the bipolar shape of the Induction-2 signals is preserved, allowing for proper treatment and reconstruction also for dense showers, as it will be shown on the real data collected with the test TPC at CERN.

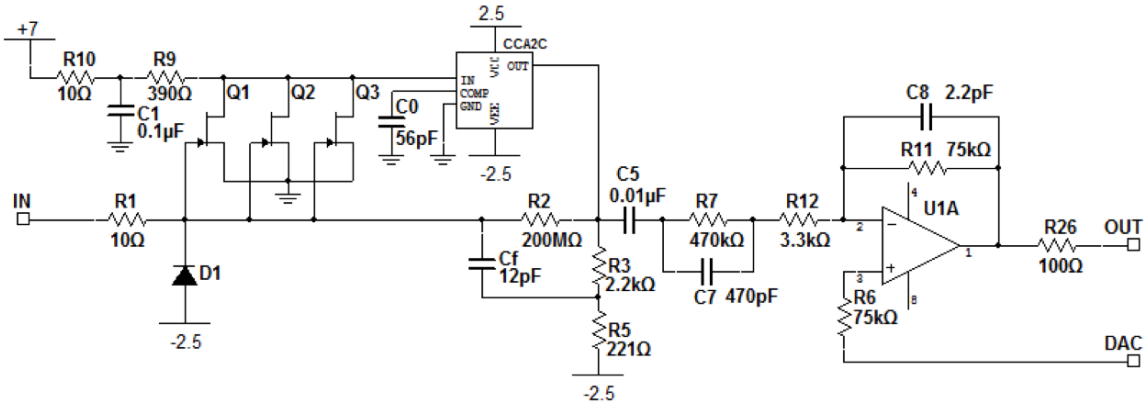

Figure 2. Front-end schematic. The high number of elements inside the BiCOMS prevents to show detailed schematic here.

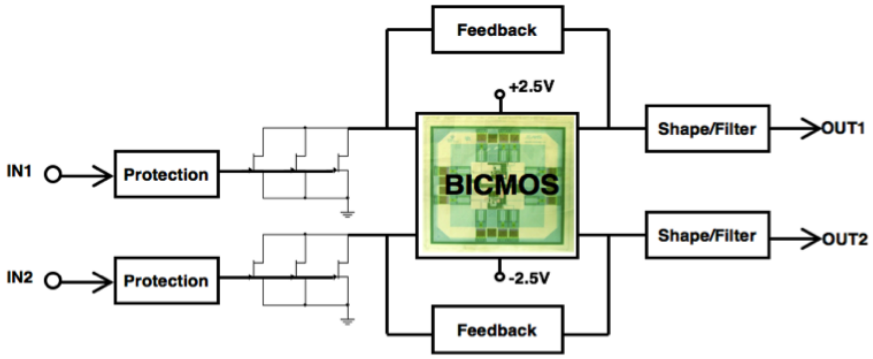

Figure 3. Block diagram of the front-end amplifier.

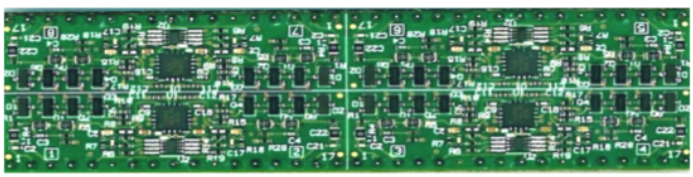

Figure 4. PCB housing 8 amplifiers with simmetrical layout.

Eight amplifiers are mounted on a single board ($81 \times 20\,\mathrm{mm}^2$) shown in figure 4 while the circuit schematic is given in figure 2. A symmetric layout for each couple of the eight channels was

2018 JINST 13 P12007

adopted to keep uniform the effects due to layout stray capacitances. Eight such small amplifier boards fit in each of the 8 connectors on the new A2795 CAEN motherboard, shown in figure 5, for a total of 64 channels. The A2795 board was designed, engineered, and built by CAEN, in collaboration with ICARUS team and according to the experiment requirements. A throughput exceeding 10 Hz was realized by a modern switched I/O system where transactions are carried out over optical 1 Gbit/s serial links. Nine motherboards are housed in a special crate mounted onto the feedthrough flange (INFN proprietary design) designed for the transmission of the TPC wire signals (see figure 10). This was an important achievement reducing the volume of the front-end electronics for each flange, serving 576 channels, from a volume of $\sim$ 600 liters of the original design (a full rack) to 10 liters.

After the pole-zero cancellation filter, in front of the serial ADC, a Bessel filter was inserted. It preserves the area (that contains the charge useful information) of the filtered signal in the passband (roll-off frequency 4 MHz) due to its linear phase response, and reduces the *rms* serial noise of 48%. Such a filter interfaces each amplifier with its serial 12 bit (Least Significant Bit LSB = 0.8 mV, 400 ns sampling time) ADC (AD7276BUJZ) mounted onto the A2795 board. A dedicated ADC for each channel avoids any multiplexing also implementing synchronous conversion. Data buffering, digital processing, and transmission onto optical link are committed to a programmable FPGA (Altera Cyclone 5 GX).

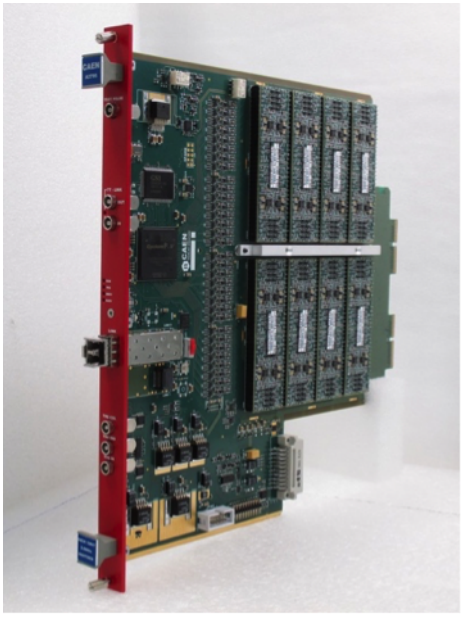

Figure 5. A2795 custom board housing 64 amplifiers (far end), AD converter, digital control, and optical link (front panel).

3 Amplifier simulations

The simulation of the new electronic chain was performed with SPICE to model its response function, gain and noise performance.

The response of the amplifier and the pole-zero cancellation filter, with zero detector capacitance (30 pF amplifier capacitance), to an injected current 100 fC$*\delta(t)$ gives an output voltage

2018 JINST 13 P12007

with a peak time $\tau = 0.6\mu s$ and amplitude of 1.64 V, where $\delta(t)$ is the derivative of the Heaviside function with dimension of [time^{-1}]. Increasing the value of the input capacitance from 30 to 500 pF would result in a corresponding reduction of the signal amplitude, as shown in figure 6 at the input and output of the Bessel filter. The simulated shaped output response is taken at the output of pole-zero cancellation where the bandwidth is around 800 kHz at the expense of a slightly reduced gain ($\sim$ 70 dB) compared with the one of the first stage integrator that has gain slightly less than 80 db, as shown in figure 7

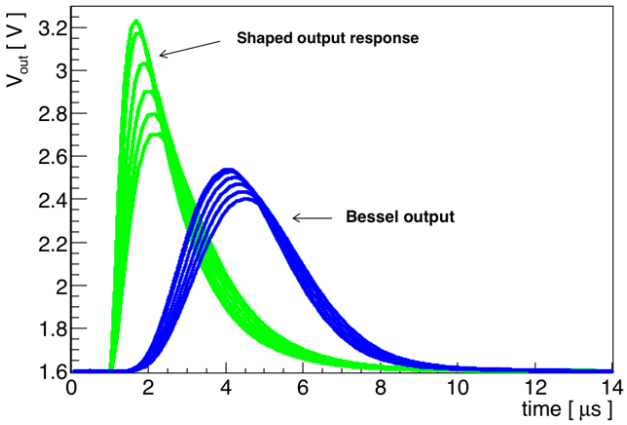

Figure 6. Shaped output response (green) at 100 fC$*\delta$(t) for Cd = 30, 100, 200, 300, 400, 500 pF, and corresponding Bessel output (blue) The area of signals, that contains the charge information, is preserved.

The amplitude reduction is due to the non-zero input impedance of the front end, $Z_{inf} \approx 600\,\Omega$. ($C_0$ / g_m C_f) in the bandwidth. However this is not relevant because the full input current will be eventually integrated as series of appropriate impulsive currents q$\delta(t)$ and the charge information will be obtained from the signal area.

The frequency response of the open loop and feedback gains (A_{OL}, A_F) of the front-end, before pole-zero cancellation, are A_{OL} = 140 db and A_F = 75 db with a 20 db/dec slope in the 50 kHz – 500 MHz range as shown in figure 7.

To interpret the simulation results we remind that the time domain response after pole-zero cancellation, to an injected current q δ(t) is

$$V_{\rm OUT}(t) = (R/\tau)q\ t/\tau e^{-t/\tau} = (q/C)xe^{-x} \tag{3.1}$$

where R and C are depending on the circuit, $\tau = 0.6\,\mu s$ and $x = t/\tau$.

The signal $V_{\rm OUT}(t)$ exhibits at $t = \tau$ the maximum value:

$$V_{\rm OUTMAX}(\tau) = R/\tau\ q/e = q/C\ 1/e\,. \tag{3.2}$$

For any kind of input current, the signal at the output of the preamplifier-shaper is the convolution of the input signal with the response function of the amplification chain:

$$V_{\rm out}(t) = \frac{1}{C}\int_{-\infty}^{t} i\,(z)\,\frac{(t-z)}{\tau}e^{\frac{-(t-z)}{\tau}}{\rm d}z\,. \tag{3.3}$$

In case of an impulsive current (e.g. that of a test pulse) $i_{tp} = q_{tp}\delta(t)$, the output signal becomes

$$V_{\rm out,tp}\,(t) = \frac{q_{tp}}{C}\frac{t}{\tau}e^{-\frac{t}{\tau}} \tag{3.4}$$

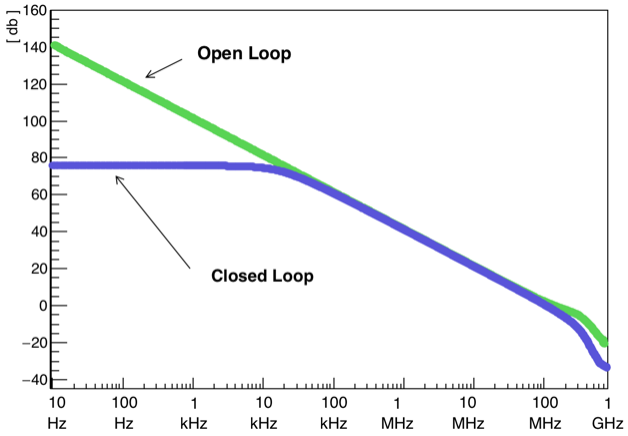

Figure 7. Frequency characteristics of the front-end integrator: open loop (green) and closed loop (blue).

and its area is proportional to the injected charge ($\int_{-\infty}^{\infty} xe^{-x}\mathrm{d}x = 1$):

$$\mathrm{Area}_{tp} = \sum_i V_{\mathrm{out,tp}}\,(i)\,\Delta\mathrm{t} = \frac{q_{tp}}{C}\int_{-\infty}^{\infty}\frac{t}{\tau}e^{\frac{-t}{\tau}}\mathrm{d}t = \frac{q_{tp}}{C}\tau. \tag{3.5}$$

Since any real input current signal recorded from the detector can be constructed as a sequence of impulsive signals with the appropriate intensity, the associated total charge can be extracted, independently from the signal shape, from the integrated area of V_{out} as:

$$\mathrm{Area}_{\mathrm{sig}} = \sum_i V_{\mathrm{out,sig}}\,(i)\,\Delta\mathrm{t} = \frac{1}{C}\int_{-\infty}^{\infty}\mathrm{d}t\int_{-\infty}^{t} i(z)\frac{(t-z)}{\tau}e^{\frac{-(t-z)}{\tau}}\mathrm{d}z = \frac{Q_{\mathrm{sig}}}{C}\tau, \tag{3.6}$$

hence as a general rule, applying test pulse calibration, the resulting charge value is:

$$Q_{\mathrm{sig}} = \mathrm{Area}_{\mathrm{sig}}\frac{q_{tp}}{\mathrm{Area}_{tp}} \tag{3.7}$$

The formula (3.7), which has been calculated after the pole-zero cancellation filter, is still valid at the Bessel output because it concerns only areas ratio and the Bessel filter has the peculiarity of preserving the shaped area.

The V_{out} signal is digitized by the ADC with LSB = 0.8 mV amplitude at 400 ns sampling time. For 100 fC input charge, at 30 pF input capacitance, the area of the output signal as calculated in the simulation is 3.18 10^{-6} Vs. Being an ADC least count area $0.8 \cdot 400\ 10^{-12}$ Vs, the 100 fC correspond to 9939 ADC elementary areas. Therefore the charge, integrated in 400 ns corresponding to 1 ADC count is:

$$q_{\mathrm{LSB}} = 0.01\ \mathrm{fC} \quad \text{or} \quad 62.5\ \text{electrons} \tag{3.8}$$

While the $\mathrm{Area}_{\mathrm{sig}}$ is 9939 ADC counts the pulse-height at the peak time is $Q_{\mathrm{peak}} = 1186$ counts. The corresponding ratio for a δ-like current, is then $9939/1186 = 8.4$. In other words, 0.8 mV peak signal is equivalent to 8.4 ADC area counts or ∼ 525 electrons. However while the collected charge is still represented by the area of the signal, the pulse-height is reduced by increasing the input capacitance as shown in figure 6, and the area-to-peak ratio shifts from 8.4 to 9.87 for an input capacitance of 30 to 500 pF respectively (figure 8).

2018 JINST 13 P12007

The RMS noise was simulated as the square root of the integral of the square power density [V^2/Hz] calculated over the bandwidth of the amplifier taking into account the cut-off due to the sampling time. The resulting Equivalent Noise Charge (ENC) as a function of the total input capacitance is shown in figure 9: the predicted noise increases with a ~ 2.5 electrons/pF slope, calculated where the serial noise is dominant. The parallel noise contributions due to the low jFet gate current (~ 0,3 pA) and 200 MΩ feedback resistor of the integrator are negligible, but included in the simulation. The current noise contribution is mainly due to the wire biasing resistor that is 10 MΩ, that is also included in the simulation.

The Bessel filter output is ±1.26 V, with a maximum input charge of ±160 fC that does not saturate the input stage for an injection time of 2 µs typical of the T600. According to the 3.3 V ADC full-scale, a total charge of ±160 fC can be managed using 76% of the 12 bit range.

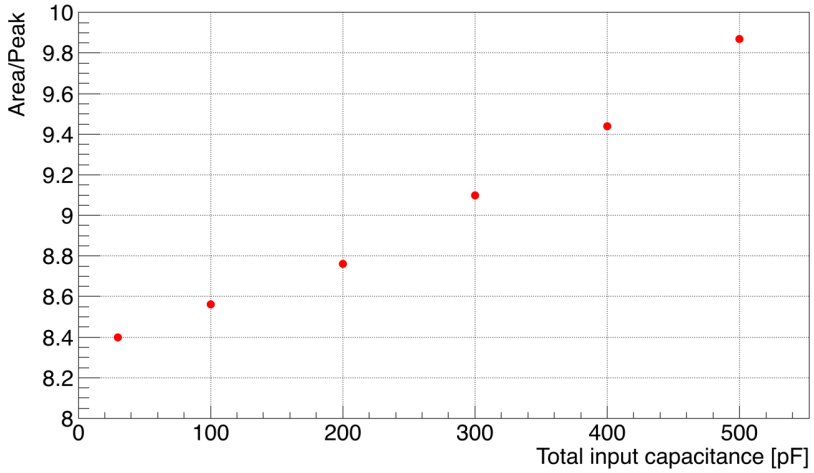

Figure 8. The simulated Area/Peak signal ratio as a function of total input capacitance.

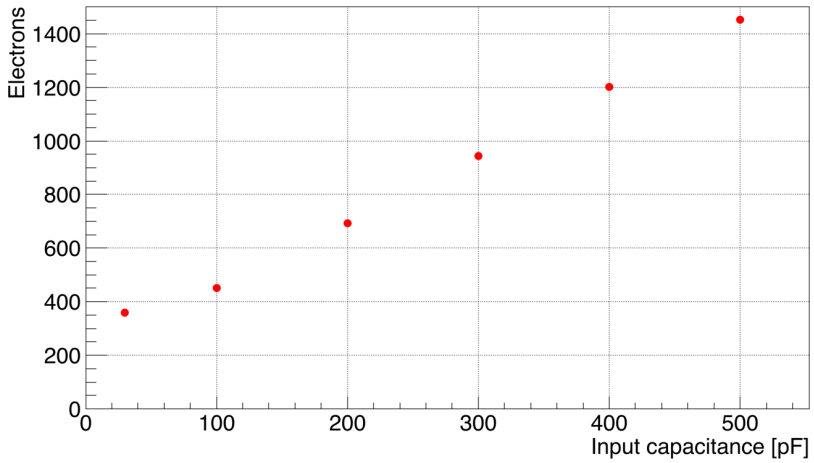

Figure 9. Simulated output ENC noise versus input capacitance.

4 Amplifier tests

Tests were performed at CERN, with the 50 liters ICARUS LAr-TPC test facility [7], characterized by a drift field of 500 V/cm on a drift length of 52 cm. The chamber is approximately $32 \times 32\,\mathrm{cm}^2$ wide and has three wire planes with 4 mm separation, 128 wires per plane, and a wire pitch $p = 2.54$ mm. The first plane (grid) facing the drift volume is not read out; the wires of the intermediate Induction are parallel to those of the grid, while those of the last Collection plane are orthogonal. The grid and the Collection planes were biased up to ±400 V (negative for grid, positive for Collection) while keeping the Induction at 0 V. The Induction and Collection wires were connected to four A2795 boards inserted in a specially designed mini-crate installed on the feedthrough flange through 2.7 m long twisted pair cables, 57 pF/m capacitance, of the type used in ICARUS-T600 (figure 10). On each board the first group of 32 channels was used for the Induction signals and the other 32 for the Collection, both read out through two optical fibers.

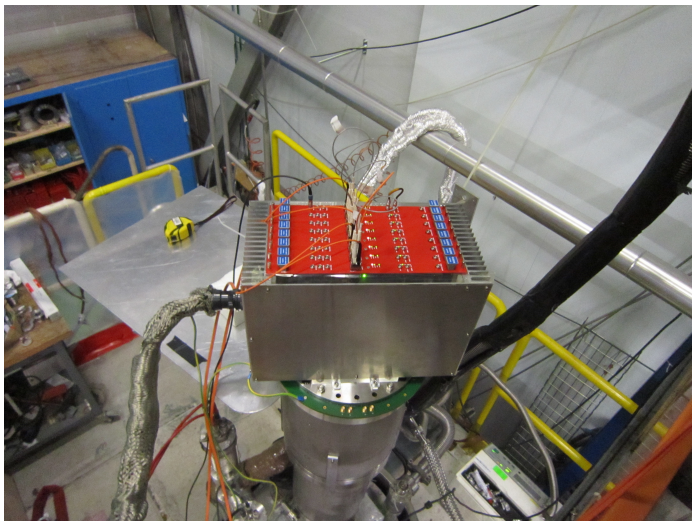

Figure 10. Test set up on the 50 liters TPC at CERN. Four of nine boards are connected to 128 Collection and Induction wires.

All the channels are equipped with a 1.75 pF (±1%) very precise test capacitance obtained with a copper strip in an inner layer of the PCB frame of the TPC wires, orthogonal to the contact tracks joining the wires to the cable connectors.

Gain and linearity of the full electronic chain, which includes the preamplifier, the shaper, the Bessel filter and the 12 bit ADC converter, were evaluated by injecting on the test capacitance fast charge pulses (0.1 µs rise time) in the 17.5–105 fC range. The resulting pulse area distribution (4732 ± 115 ADC counts) is shown as a function of the channel number in figure 11 for an injected charge of 52.5 fC (327600 electrons). The gain turns out $q_{LSB} = 69.2 \pm 1.7$ electrons /ADC count to be compared with the 62.5 electron/ADC count as predicted by the simulation, the 2.5% uncertainty reflecting the small non-uniformity of the electronic chain. The signal area was verified to be constant at 2% level by injecting test pulses with rise time in the 0.1–4 µs range (figure 12).

2018 JINST 13 P12007

In conclusion the total charge of any signal Q_{tot} is then given by

$$Q_{\text{tot}} = \sum_i q_{\text{LSB}} \text{ADC}_i \tag{4.1}$$

where ADC_i is the ADC count at the i-sample.

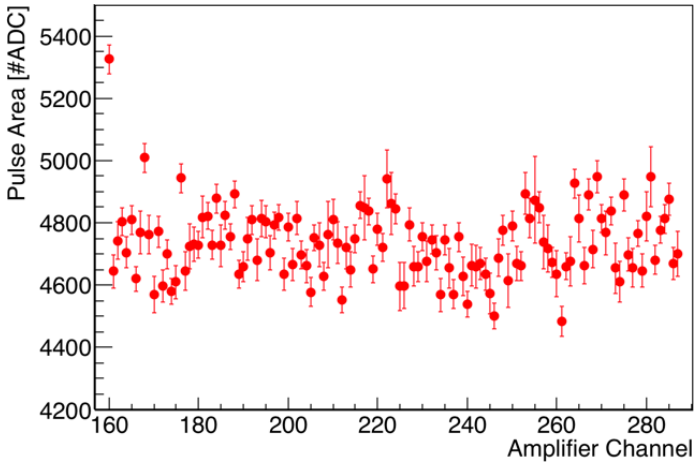

Figure 11. Pulse area as a function of the amplifier channel in Collection view (52.5 fC injected charge, 0.1 µs risetime).

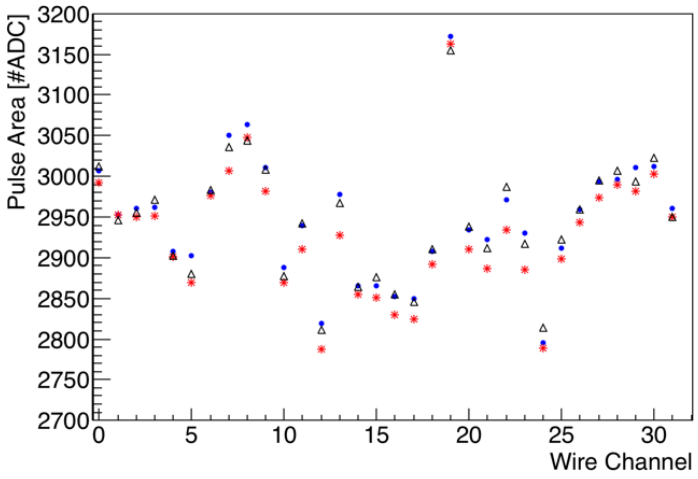

Figure 12. Pulse areas on 32 channels (Collection view) at three different rise time input signals (0.1, 2.0 and 4.0 µs in red, blue, black respectively) for 32 fC injected charge.

Finally, the injection of δ-like charge pulses in the 17.5 fC – 105 fC range allowed to verify the gain linearity within 0.5%, and to test the linear relation between the total charge Q_{tot} (signal area) and the signal pulse-height Q_{peak} (see figure 13), resulting in

$$Q_{\text{tot}} = 7.7 Q_{\text{peak}} \,. \tag{4.2}$$

The measured 7.70 ± 0.06 ratio is consistent with the ∼ 8.6 simulated value for the ∼ 130 pF total input capacitance, including the cables, as quoted in figure 6. We could explain this and

2018 JINST 13 P12007

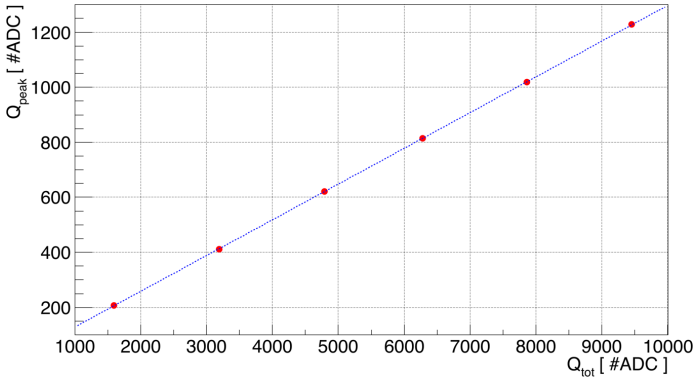

Figure 13. Q_{peak} versus different δ-like input charges Q_{tot}.

following discrepancies to the fact that in the experimental set-up (like in the real full size detector) there is an inherent cross talk among signal wire planes that attenuates in fact both injected and physical signals.

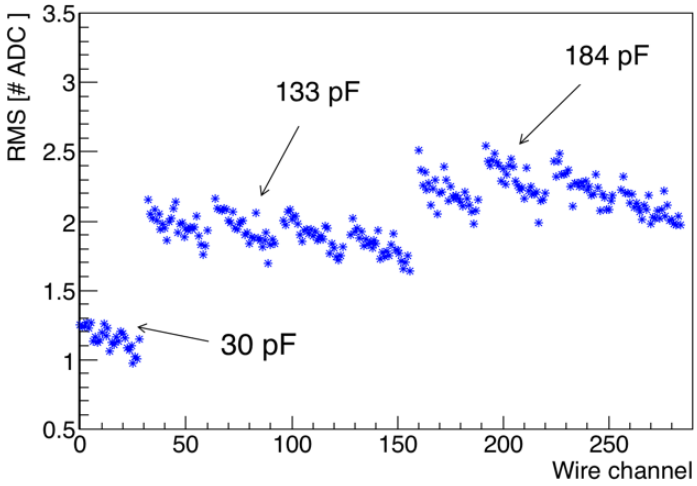

Figure 14. RMS noise in ADC counts for the three input capacitance configurations as described in the text.

Noise measurements were performed in three set-up conditions, characterized by different input capacitances (figure 14): 30 pF (JFet only), 133 pF and 184 pF as introduced by the addition of 1.8 m and 2.7 m cable length respectively. A clear channel-to-channel noise pattern regularly repeating in each board, related to the A2795 layout, is recognized where the baseline of this is not easy to evaluate. A coherent noise on each board, visible as a texture in the event images (see for example figure 16 and figure 17), was evaluated from the average, for each time sample, of the 32 wire waveforms in the same board (table 1). This effect is due to the mother board layout and to the fact we were testing our system in a real experimental hall with its intrinsic limitations in terms of coherent noise.

For sake of comparison with the single channel simulation, the contribution to the noise introduced by the A2795 layout was removed by selecting the least noisy channel in each board (column 4 of table 1). After subtracting in quadrature the coherent contribution from the value associated to this channel (Column 5 of table 1) the intrinsic noise of a single channel is obtained

2018 JINST 13 P12007

Table 1. RMS noise measurements (pulse-height) for the three different input capacitances quoted in the text. Column 3: average noise over 64 channels in a board; Column 4: the minimum noise averaged over the boards with the same Cd; Column 5: average coherent noise; Column 6 and 7: intrinsic channel noise, to be compared with simulation. The conversion factors in column 2 are determined from figure 8 taking into account relation (3.8).

Cd (pF)	Conversion factor	Electronic noise				
	Electrons/ADC peak count	Average (counts)	Minimum (counts)	Coherent (counts)	Intrinsic (counts)	Intrinsic (electrons)
30	525	1.15 ± 0.08	1.08 ± 0.04	0.32 ± 0.02	1.03 ± 0.04	541 ± 21
133	539	1.90 ± 0.11	1.82 ± 0.06	0.81 ± 0.05	1.63 ± 0.08	879 ± 43
184	546	2.21 ± 0.13	2.13 ± 0.08	0.98 ± 0.07	1.89 ± 0.11	1032 ± 60

(column 6, 7 of table 1). Both the average and intrinsic measured noise are shown in figure 15 as a function of the total input capacitance. A noise slope of ∼ 3.6 electrons/pF in the measurements, calculated where the serial noise is dominant and reduced to ∼ 3 electrons/pF for the intrinsic noise contribution, has to be compared with ∼ 2.5 electrons/pF value obtained from the simulation.

While the board layout effects and coherent noise cannot be included in the simulation, the results in table 1 provide a reasonable picture of the front-end electronics from the point of noise slope. We can only conclude that we cannot fully simulate the effects of the detector geometry. However this effect does not impact with the purpose of the physics measurements.

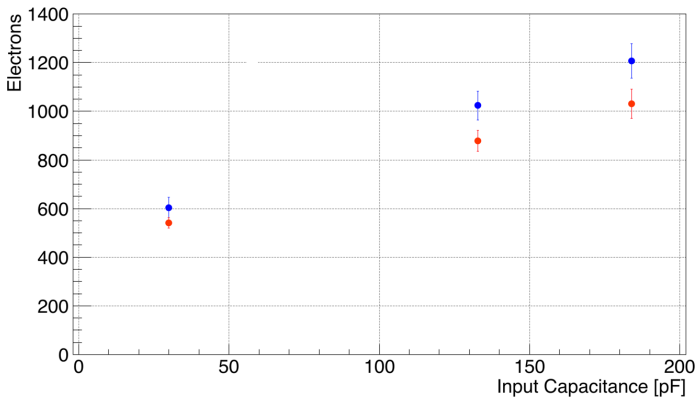

Figure 15. Noise slope for the three quoted input capacitances: blue and red values refer to average and intrinsic noise respectively as quoted in table 1.

According to the 3 mm wire pitch and plane spacing of ICARUS-T600, a signal to noise ratio S/N ≈ 15000/1200 ∼ 12 can be roughly expected for ∼ 15000 electrons signal released on a single TPC wire by a m.i.p. particle in 3 mm LAr [5].

5 Tests with cosmic rays

Cosmic ray events were collected at CERN with the 50 liters ICARUS LAr-TPC equipped with the new electronics, at the nominal drift field of 500 V/cm. An external trigger was set up based on the

2018 JINST 13 P12007

coincidence of two external plastic scintillator slabs and an internal Hamamatsu 8" photomultiplier coated with TPB wavelength shifter [5]. It selected mainly cosmic muon tracks inclined at about 45° with respect to the drift direction, spanning most of the wires in both the Induction and Collection planes (an example is shown in figure 16). Moreover a fraction of the triggered events consisted of electromagnetic showers (figure 17) induced by cosmic rays.

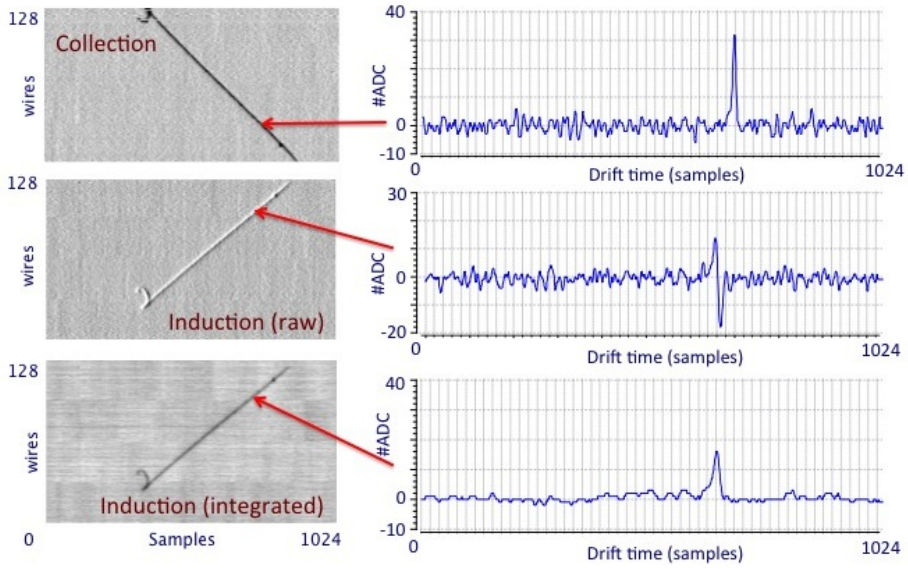

Figure 16. Example of single muon tracks at ~ 45° with respect to the drift direction collected with the 50 liters ICARUS LAr-TPC and the new electronics with ±400 V bias in Collection and grid wires. Induction signal is shown as raw data as well as after integration and filtering to recover unipolar features. The corresponding waveforms recorded on one channel are also reported on the right.

Muon tracks were used to calibrate the electronic chain with minimum ionizing particles. Measurements were performed to reach an almost full transparency to the drifting electrons for both the screen grid and the Induction plane by varying the biasing voltage in the ±275, ±400 V range on the screen grid and the Collection plane while keeping the induction plane at 0 V. Landau dE/dx distributions of the charge deposited in LAr by minimum ionizing particles (dE/dx ~ 2.1 MeV/cm in LAr) were obtained (figure 18) by selecting through-going muon tracks reconstructed in 3D and calculating the signal area on the wires of the Collection plane with the previously described procedure. Small corrections, due to finite electron lifetime, were also introduced as measured from the same muon track sample.

The transparency of both the screen grid and Induction plane was determined as a function of the biasing voltage by studying the most probable value of the muon dE/dx Landau distribution, scarcely affected by track inclination and dE/dx relativistic rise. An almost full grid transparency is reached at 400 V for which the collected charge is ~ 76 (ADC counts)/mm (figure 19).

At the nominal drift field of 500 V/cm the electron-ion recombination parameter is ~ 0.7 as measured by ICARUS at LNGS [4]. The dE/dx most probable value of 1.75 MeV/cm corresponds to 0.85 fC/mm. As a consequence, the electronic calibration of signal on Collection was measured

2018 JINST 13 P12007

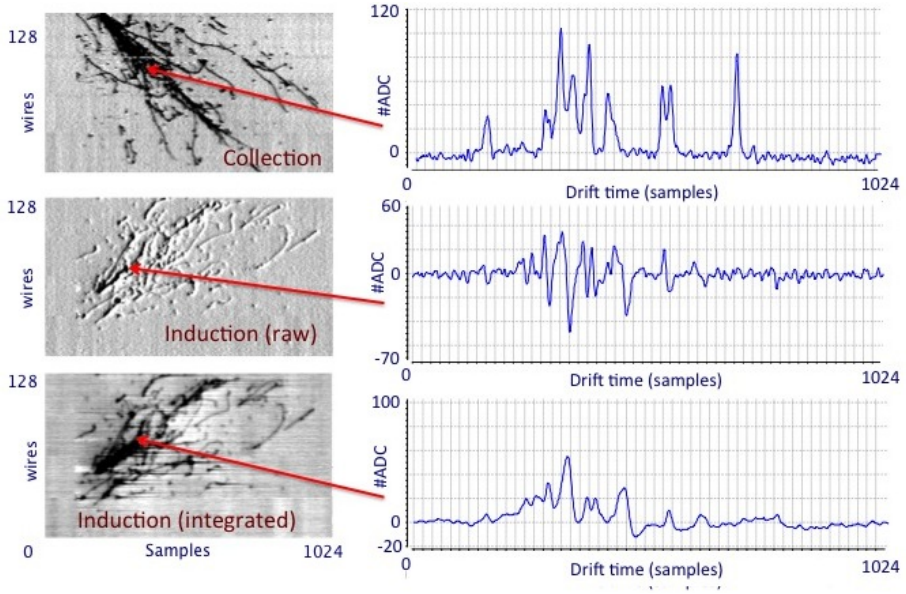

Figure 17. Example of multi-prong event (electromagnetic shower) collected with the 50 liters ICARUS LAr-TPC and the new electronics with ±400 V bias in Collection and grid wires. Induction signal is shown as raw data as well as after signal integration to recover unipolar features. A corresponding waveform signal recorded on one channel is reported on the right.

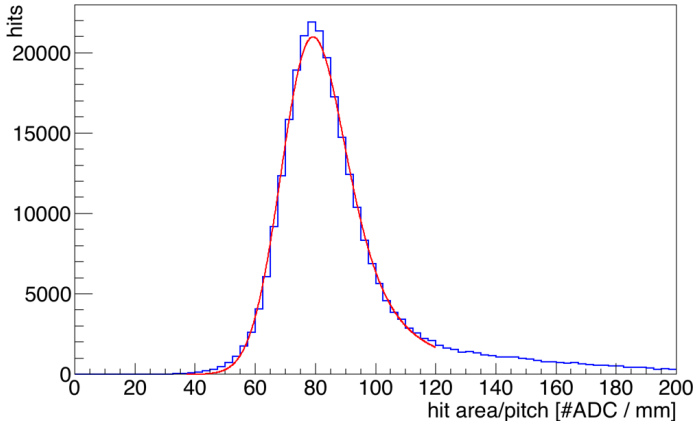

Figure 18. Example of Landau dE/dx distribution from through-going muon tracks as measured on the Collection plane as fitted with a Landau-Gaussian convolution (±400 V/cm biasing voltage). The most probable value is 76 #ADC/mm. The width of the distribution, evaluated from the RMS of the fitting Gaussian and the scale parameter of the fitting Landau added in quadrature, result 12% of the most probable value, in agreement with the Landau and the electronic noise fluctuations.

to be:

$$C = 0.85\,\mathrm{fC/mm}/76(\mathrm{ADC\ counts/mm}) = 0.011\,\mathrm{fC/ADCcounts}(\sim 69\ \mathrm{electrons/ADC}) \quad (5.1)$$

in agreement with both test pulse data (69.2 ± 1.7 electrons/ADC count) and simulations (62.5 electrons/ADC count).

2018 JINST 13 P12007

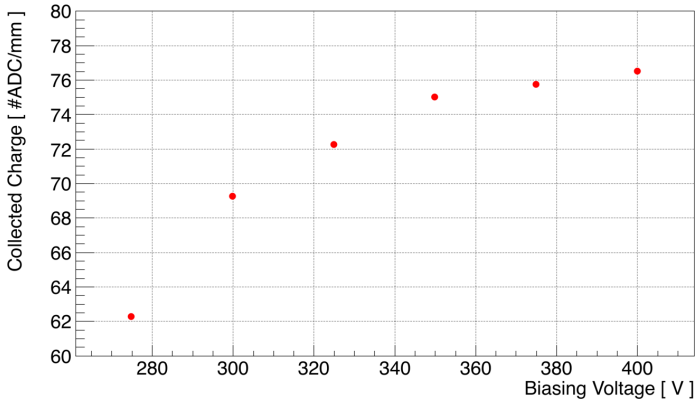

Figure 19. The most probable value of the dE/dx distributions from through-going muon tracks as measured on the collection plane as a function of the wire planes biasing voltage.

While the Collection signal is simply proportional to the current i(t) collected on the wire at a given time, the bipolar nature of the Induction signal requires a specific treatment in order to extract a signal proportional to the charge. The Induction signal origins from both the contribution of the electron cloud approaching the Induction plane at a time t, and the one drifting away from the Induction wires, i.e. the incoming electrons at a previous time t-Δt, where Δt is the transit time between the two wire planes. An unipolar signal similar to the Collection one is obtained by integrating this differential signal over time and normalizing it for the average transit time Δt; the charge sensed by the Induction wires can be then recovered by a second integration. This two steps procedure, however, would enhance the low frequency noise components, requiring an additional filtering for the charge measurement.

As a first possible implementation of this scheme, a running sum integration of the Induction signal was performed followed by a baseline restoring based on the difference between the integrated signal itself and its average over $\sim$ 30 μs, a much longer time scale compared to the few μs signal duration. The normalization factor $\Delta t \sim 4\,\mu$s has been obtained from the average duration of Induction signals, after correcting for the track inclination. The outcome of this process is shown in the bottom images of figure 16, figure 17.

The adoption of the new optimized preamplifier in the front-end for both Induction and Collection wires with a fast signal shaping time to match the electron transit time in the wire spacing, prevents the signal undershoot as well as reducing the low frequency noise. The obtained unprecedented event image sharpness with an improved hit separation allows to resolve crowded and complex events both in Collection and Induction views. The recorded muon track (figure 16) shows an average peak signal to RMS noise ratio S/N $\approx 30/2.2 \sim 14$ and S/N $\approx 15/1.5 \sim 10$ in Collection and Induction views after integration and filtering. The obtained values would further increase for ICARUS-T600 if the 3 mm different wire pitch and wire plane separation are accounted for. By a term of comparison, even if the bipolar treatment of the Induction signals prevents a completely homogeneous comparison, the corresponding S/N ratios as measured in T600 with the previous front-end electronics for similarly inclined muons were $\sim$ 14 in Collection and $\sim$ 7 in Induction.

As an initial evaluation of the potentialities of the dE/dx measurement in the Induction plane, the Landau distribution of the charge sensed by the Induction wires has been computed for the

2018 JINST 13 P12007

collected muons (figure 20). The difference between Collection and Induction pulse areas is mainly due to the fact that only ~ 70% of drifting electrons charge is expected to be sensed on induction wires due to the geometry of the detector; a further small reduction of the signal height is due to the filtering procedure. The larger width of the distribution is attributed to the not fully filtered low frequency noise.

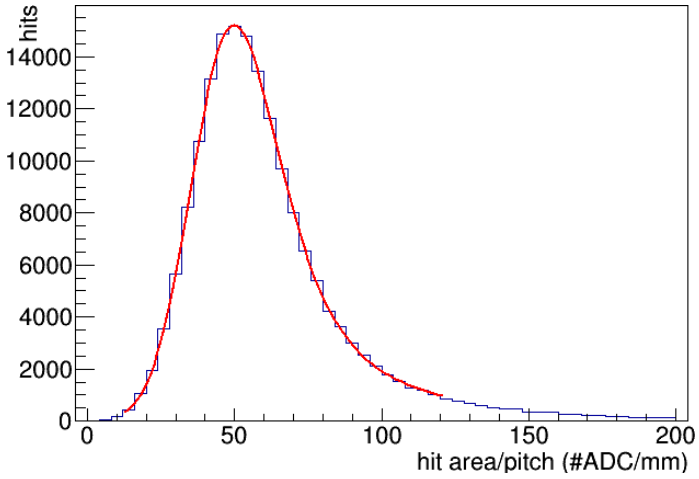

Figure 20. Example of Landau dE/dx distribution from through-going muon tracks as measured on the Induction plane, fitted with a Landau-Gaussian convolution. Biasing voltage is ±400 V/cm. The most probable value is 45 # ADC/mm. the percent width of the distribution as defined in figure 15, is ~ 24%.

6 Conclusions

The new read-out electronics for ICARUS-T600 liquid argon TPC prepared in view of its operation in Fermilab on SBN beam includes a new design front-end, a serial 12 bit ADC system (one per channel) and serial bus architecture with optical links for Gigabit/s data transmission. In the new compact set-up both the analog and digital electronics are hosted directly on ad-hoc signal feed-through flange acting as electronic back-plane. The digital part is fully contained in a single high-performance FPGA in each board handling the ADC data. The same new preamplifier was adopted in the front-end for both Induction and Collection wires, with a faster shaping time to match the electron transit time in the wire plane spacing. Globally the throughput of the read-out system exceeds 10 Hz with optical Gigabit/s serial links.

The new ICARUS electronic chain was successfully tested with the 50 liters LAr-TPC exposed to cosmic rays. Beside its already well-established performance in the charge Collection wires a more efficient handling of signals in the intermediate Induction 2 wire plane with a significant increase of S/N was measured. The optimized preamp architecture resulted in unprecedented image sharpness of the events, with a better hit signal separation even in crowded and complex events like electromagnetic showers, both in Collection and Induction views.

The use of dedicated algorithms for the bipolar signals from Induction wires allows for measuring energy deposition in Induction view also, with a $\Delta E/E \sim 24\%$ resolution on the single hit. At low energy Booster neutrino beam this feature will enable the recovering of leading lepton tracks travelling along the Collection wire direction for which the signal cannot be fully exploited for the

2018 JINST 13 P12007

dE/dx analysis and particle track separation, with an expected significant increase of the electron neutrino reconstruction efficiency [7].

Acknowledgments

This work was funded by INFN in the framework of WA104/NP01 program finalized to the overhauling of ICARUS detector in view of its operation on SBN at Fermilab. The A2795 board was designed, engineered, and built by CAEN, in collaboration with ICARUS team and Electronics Service facilities of INFN, Padova. The strong contribution of A. Mati and A. Romboli from CAEN was essential.

References

[1] C. Rubbia, *The Liquid Argon Time Projection Chamber: A New Concept for Neutrino Detectors*, CERN-EP-INT-77-08.

[2] C. Rubbia et al., *Underground operation of the ICARUS T600 LAr-TPC: first results*, 2011 *JINST* **6** P07011 [arXiv:1106.0975].

[3] M. Antonello et al., *Experimental observation of an extremely high electron lifetime with the ICARUS-T600 LAr-TPC*, 2014 *JINST* **9** P12006 [arXiv:1409.5592].

[4] A. Ankowski et al., *Characterization of ETL 9357FLA photomultiplier tubes for cryogenic temperature applications*, *Nucl. Instrum. Meth.* **A 556** (2006) 146.

[5] ICARUS collaboration, S. Amerio et al., *Design, construction and tests of the ICARUS T600 detector*, *Nucl. Instrum. Meth.* **A 527** (2004) 329.

[6] ICARUS collaboration, M. Antonello et al., *Experimental search for the "LSND anomaly" with the ICARUS detector in the CNGS neutrino beam*, *Eur. Phys. J.* **C 73** (2013) 2345 [arXiv:1209.0122]; ICARUS collaboration, M. Antonello et al., *Search for anomalies in the ν_e appearance from a ν_μ beam*, *Eur. Phys. J.* **C 73** (2013) 2599 [arXiv:1307.4699] [INSPIRE].

[7] LAr1-ND, ICARUS-WA104 and MicroBooNE collaborations, M. Antonello et al., *A Proposal for a Three Detector Short-Baseline Neutrino Oscillation Program in the Fermilab Booster Neutrino Beam*, arXiv:1503.01520.

[8] ICARUS-Milano collaboration, F. Arneodo et al., *Performance Of A Liquid Argon Time Projection Chamber Exposed To The WANF Neutrino Beam*, *Phys. Rev.* **D 74** (2006) 112001 [physics/0609205].

2018 JINST 13 P12007